Particle motions in oscillatory flow over a smooth bed

Jensen, Karsten Lindegård; Sumer, B. Mutlu; Fredsøe, Jørgen; Hjelmager Jensen, Jacob

Published in:
Book of Proceedings

Publication date:
2014

PARTICLE MOTIONS IN OSCILLATORY FLOW OVER A SMOOTH BED

KARSTEN LINDEGÅRD JENSEN(1), B. MUTLU SUMER(1), JØRGEN FREDSØE(1) & JACOB HJELMAGER JENSEN(1)

(1) *Technical University of Denmark, Dept. of Mech. Engineering, Kgs. Lyngby, Denmark, klije@mek.dtu.dk*

Abstract

This study investigates particle motions near the bed in an oscillating tunnel with a smooth bed. Trajectories of a heavy particle were recorded in two dimensions (horizontal and vertical) and in time. The wave boundary layer Reynolds number is Re = 520000. Kinematical quantities such as the probability distribution of particle position in the vertical, and the horizontal and vertical particle velocities, among others, are determined. The particle is observed to reach heights of 2.5-3d, similar to that characterizing a typical bedload particle in sediment transport.

Keywords: oscillatory flow; particle tracking; sediment transport; single particle, turbulence;

1. Introduction

The motion of single particles have been studied extensively over the years see e.g. Grass, 1974; Sumer and Oguz, 1978; Sumer and Deigaard, 1981; Niño and Garcia, 1996. These investigations have been undertaken in steady flows. To the authors' knowledge, no experimental study is yet available, investigating the particle motions in wave (or oscillatory) boundary layers. The present investigation extends the previous work to oscillatory boundary layer flows. The quantities related to particle motion in the present case such as the probability distribution of particle position in the vertical (equivalent to the sediment concentration in the Eulerian approach), the horizontal and vertical particle velocities, and several other related statistics are, now, a function of phase. Unlike the real sediment, the unique advantage of using the single particle approach is that the experiments can be conducted under controlled conditions. Also equally important, the single particle approach enables one to get a better insight into the processes governing the sediment transport.

2. Experimental setup

The experiment has been conducted in an oscillating water tunnel with a 10 meter long working section and a cross section of 39 cm x 29 cm (width x height), Figure 1. The tunnel is the same as that used in Jensen, Sumer and Fredsøe, 1989. The period T of the flow is 9.72 s, which corresponds to the natural period of the tunnel. The particle tracking is performed in the center of the working section based on a recording with 50 frames per second (fps) by a digital camera recording in full HD (1920 times 1080 pixels).

The experiments are carried out in dark, the camera and tunnel being covered with black cloth. Only the center of the tunnel where the particle is tracked is illuminated by a light sheet. The light sheet is made by LED spots placed in the top of a 60 cm high and 3 cm wide box, Figure 1. Although the light sheet is 4 cm in width on the bed, the inclination of the side surface of the light sheet is only 0.7˚ so the width of the light sheet near the bed (where the particle travels) is

approximately constant. Furthermore, the box is painted black inside to absorb the light so that the light sheet only consists of the light emitted from the spots. This ensures a well and sharply defined light sheet so that the particle is illuminated when it is in the light sheet, and it is not otherwise. The particle tracking is only done in two dimensions (vertical (y) and horizontal (x)) so the width of the light sheet is a trade-off between the accuracy in the transverse direction and how often the particle is present in the light sheet. Ideally, a relatively thinner light sheet should have been used, but since the flow in the boundary layer is three dimensional the time the particle would stay in this thin light sheet would have been too small, meaning that it would have required too many waves to obtain reliable ensemble averages. We note that the present light sheet leads to an error in the calibration of the length scale. This is because the distance from the camera to the particle varies within the light sheet in the transverse direction. This error is determined and is found to be less than ±1 %, however.

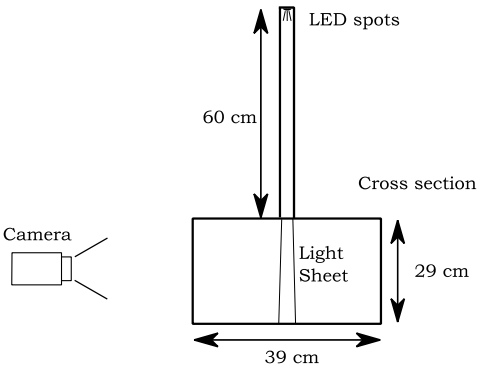

Figure 1 camera and light sheet arrangement.

The procedure used in the experiments is as follows: (1) Fill the tunnel, (2) Inject the particle into the tunnel. This is through a double valve in the lid of the tunnel. (3) Let the particle settle on the bed. (4) Run the tunnel for 10 waves (warm-up period), with the particle already set into motion. The latter is to avoid the influence of the initial particle position on the end results. (5) Start recording the trajectory of the particle.

During the test the free stream velocity, $U_{0m,}$ is recorded with a LDA (Laser Doppler Anemometry). The camera recording and velocity measurements are synchronized with the help of a voltage signal resulting in a flash in the video, and a peak in a separate channel in the data file for the velocity. Before each test, the water temperature is measured in order to secure the same conditions for each repetitive run of the experiments.

2.1 Test conditions

The test conditions are listed in Table 1. The test has been run for 660 periods in total, because the particle position cannot be controlled. The sampling frequency was 50 Hz and for each sampling time the particle positions have been determined in minimum 60 different waves. The Reynolds number, Re, is 520000 where $\mathrm{Re} = aU_{0m}/\nu$, ν is the kinematic viscosity, and a is the amplitude of the motion $a = U_{0m}T/(2\pi)$ in which U_{0m} is the maximum value of the flow velocity defined by

$$U_0 = U_{0m}\sin(\omega t) \qquad [1]$$

in which U_0 is the flow velocity in the free-stream region, t is time and ω is the angular frequency of the flow, $\omega=2\pi/T$.

The friction velocity, U_f

$$U_f = U_{fm} f(\omega t + \phi) \quad [2]$$

has been measured directly with a hot film probe (see Section 2.3) in which U_{fm} is the maximum value of the friction velocity, and φ the phase lead with respect to the free stream velocity. U_{fm} of the present test is measured to be U_{fm} = 2.5 cm/s, in complete agreement with Jensen et al., 1989.

Table 1. Test condition. Reynolds number Re = aU_{0m}/ν, a = $U_{0m}T/(2\pi)$, T_{water} the water temperature.

T [s]	U_{0m} [cm/s]	a [cm]	Re	U_{fm} [cm/s]	T_{water} [°C]
9.72	60	92	520000	2.5	18

The particle properties are listed in Table 2. The spherical-shape particle, the size, d, of 2.95 mm is printed on a 3D printer, each layer printed being 16 μm thick. The specific gravity of the particle is $s = \gamma_s/\gamma$ = 1.23 in which γ_s is the specific weight of the particle and γ the specific weight of water. The settling velocity, w, has been measured in a 1.5 meter high water column, and after the particle reaches terminal velocity the time and the distance travelled by the particle is recorded with a video camera. The test is repeated to get a sample of 30 realizations, and the fall velocity is determined over this sample. The settling velocity parameter is defined by $w/(\kappa U_{fm})$, where κ is Karman constant (0.41). In the definition of the settling velocity parameter the maximum value of the friction velocity is used rather than the phase-resolved values of U_f, and this is for simplicity.

Table 2. Particle properties. d is the particle diameter, dU_{fm}/ν is the grain Reynolds number, w the fall velocity, s the specific gravity of the particle and $w/(\kappa U_{fm})$ the settling velocity parameter.

d [mm]	dU_{fm}/ν	w [cm/s]	s	$w/(\kappa U_{fm})$	θ
2.95	70	10	1.23	10	0.094

Regarding the particle parameters, the way in which the particle is transported deserves an early discussion. As seen from Table 2, the settling velocity parameter $w/(\kappa U_{fm})$, is larger than unity, and therefore the particle cannot be maintained in suspension. However, as the particle grain Reynolds number, dU_{fm}/ν, is substantially larger than the thickness of the viscous sublayer, $dU_{fm}/\nu = 70 > 5$, meaning that the particle is fully exposed to the main body of the fully developed turbulent boundary layer flow, and furthermore because of the large value of the Shields parameter, $\theta = U_{fm}^2/(g(s-1)d) = 0.094$, the particle (which cannot be maintained is suspension) is expected to move near the bed (1) by rolling on the bed in the beginning of the flow half cycle, and (2) subsequently, hoping into the flow with increasing flow velocity during the half cycle. In this latter stage, the particle is expected to hop into the flow repeatedly as it returns back to the bed, in a series of leaps, as revealed by the experimental trajectories, Figure 2.

2.2 Velocity measurement

The velocity is measured with a two component LDA from Dantec Dynamics. The laser was used in the backscatter mode. The LDA was, in the present study, used for several purposes, namely to monitor the free stream velocity, to measure the velocity profile across the depth of the boundary layer, and to determine the direction of the flow just above the hot film probe (as the hot film probe cannot sense the direction). For the velocity profile, a total of 50 waves were sampled. The number of waves required to get reliable ensemble averages has been discussed in greater details in Sleath, 1987, and Jensen et al., 1989.

2.3 Bed shear stress measurement

The bed shear stress was measured directly with a hot film probe from Dantec Dynamics (type 55R46) which is flush mounted to the tunnel bed. The hot film probe is calibrated based on the shear stress in the laminar wave boundary layer where the shear stress is known, so the calibration coefficients A and B in the calibration relation in Eq. 3 can be determined from (Hanratty and Campbell, 1982):

$$\tau^{1/3} = AE^2 + B \qquad [3]$$

For further description of the hot film technique, see e.g. Sumer, Arnskov, Christensen and Jørgensen, 1993 or Carstensen, Sumer and Fredsøe, 2010.

2.4 Particle tracking

The following paragraph describes the principle ideas in the particle tracking. The particle tracking and image processing is performed in Matlab. First the video is split into single frames that are gray scaled. Then the particle tracking starts with identifying the particle on the image based on limits for (1) the light intensity the particle has in the image, (2) size of the particle and (3) eccentricity. These limits help to remove any unwanted noise or objects from the image. This can occur if e.g. a coarse sand grain is present in the light volume and thereby creating a reflection which is captured by the camera. The second step in the particle tracking is to combine the individual particle positions so that a trajectory can be made by specifying the maximum distance the particle can move between two frames. If two or more positions exist in the second frame then the new position of the particle cannot be determined and therefore the trajectory is discarded.

After the trajectory is obtained the particle positions are corrected for distortion and scaled so that the trajectory is in length units. The last thing is to correct for the wave phase and then the statistical process can begin. All the positions are for the centroid of the particle.

3. Results

3.1 Flow

To compare the particle velocity with the flow velocity, velocity profiles have been measured.

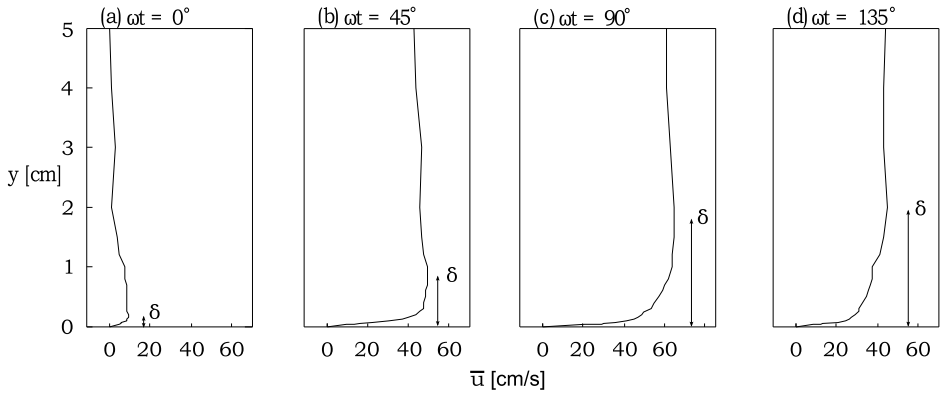

Figure 2. The vertical velocity profile for ωt = 0˚, 45˚, 90˚, 135˚ and 180˚ measured by LDA. The boundary layer thickness, δ, develops as ωt increases. The definition of δ follows Jensen et al., (1989 Figure 24).

Figure 2 shows the velocity profiles for ωt = 0˚, 45˚, 90˚ and 135˚. The boundary layer thickness, δ, defined according to Jensen et al., (1989 Figure 24), is also shown in Figure 2. For ωt = 90˚ δ = 1.8 cm. In Figure 2a the phase lead for the near bed flow can be seen. It has been determined to 12˚. Both are in agreement with the results by Jensen et al. 1989.

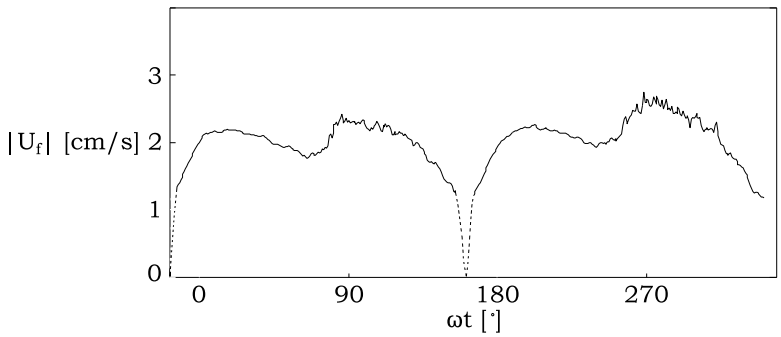

Figure 3. The Absolute value of flow resistance in terms of the friction velocity U_f as function ωt. Notice the double peak in the friction velocity. This double peak in each half period was also found by Jensen et al., 1989 and Hino et al., 1976

The flow resistance in terms of the absolute value of U_f is shown in Figure 3. Each half cycle has a double peak in the friction velocity, as reported by Jensen et al., 1989, for this particular Reynolds number, and earlier by Hino, Sawamoto and Takasu, 1976.

Finally, the flow is, according to Jensen et al., 1989, in the transitional regime after ωt = 30˚ and in the fully developed turbulent regime after ωt = 100˚.

3.2 Particle path and pdf

The test is conducted with a single spherical particle over a smooth bed. Therefore the particle being on the bed is exposed to the flow and as a consequence of this it will start to roll immediately as the flow velocity is increased.

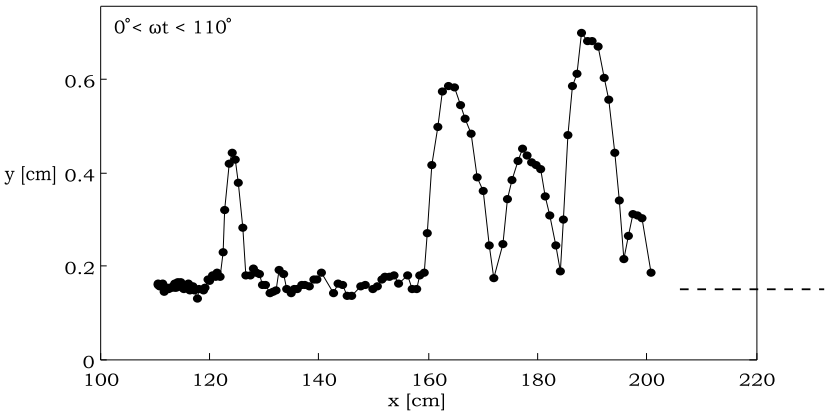

Figure 4. Typical particle path. Horizontal dashed line coincides with the centroid of the particle when it is on the bed. This examples covers a phase interval of 0° < ωt < 110°. The bed is located at y= 0. The particle moves from left to right. Notice the jumps up into the flow both for small values for ωt (at x = 125 cm) and for larger values around maximum velocity (x = 180 cm). Note that the time between the dots is 0.02 s or 0.7°. Furthermore, the dots represent the center of the particle.

Figure 4 displays a typical particle trajectory. The record covers the time period 0° < ωt < 110° in which the lower bound ωt = 0° corresponds to the phase where the flow velocity in the free stream is nil, and the upper bound ωt = 110° to a phase slightly after the phase where the flow velocity becomes maximum (ωt = 90°). From time to time, the particle hops into the flow and other times it stays near the bed and only experiences small jumps before it settles again.

Figure 5 shows the frequency histograms representing the probability density function (pdf) of particle position in the vertical for values of the phase ωt = 0°, 45°, 90°, …, covering one flow period. The vertical intervals are chosen to be half of the particle size, $d/2$, for convenience, starting from 0.1 cm. Around the flow reversals (Figures 5(a) and (e)), the particle is mainly near the bed. In Figure 5(a) the particle may reside also in interval number 2 from the bed. This is due to the following reason. The particle from time to time around flow reversals is caught by the vortex created by the inflection point and lift from the bed shortly before it settles again. The measurement precision in determining the position of the particle may also affect the end results, because if the distance the particle moves between two successive images is small an error in the determination of the centroid may occur. This error will then lead to a velocity based on the two images dominated by the error in the determination of the centroid. Therefore high accuracy is desired in determining the centroid. In the present case the centroid is determined with an accuracy of maximum 0.5 pixel or 0.55 mm.

As the phase progresses, the frequency histograms start to show values higher up in the flow and lower occurrence near the bed. As already discussed, the settling velocity parameter ($w/(\kappa U_{\mathrm{fm}})$ = 10) is so large, however, that the particle cannot be maintained in suspension, and therefore it returns to the bed after it has been brought into "suspension".

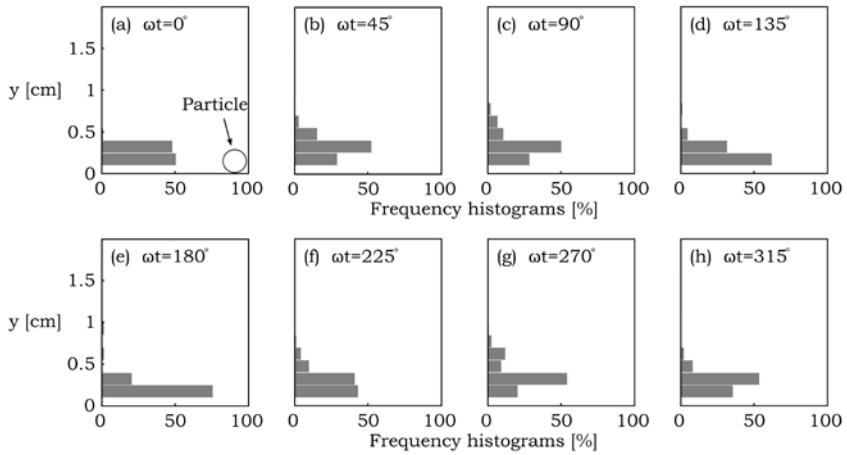

Figure 5. Frequency histograms for particle position for selected values of ωt. Circle representing the particle in (a) is added as a scale. The intervals at the histograms are chosen to be half of the particle size, $d/2$, starting at 0.1 cm.

Furthermore, Figure 5 shows that the particle can be characterized as bedload since it moves up to 2.5d-3d from the bed, which, again, is due to the large settling velocity parameter. It should be noted that, in the upper intervals, the number of samples can be as low as 1 to 4 samples in the interval (b) between 0.55 and 0.7, (c) between 0.55 and 0.7 and again between 0.7 and 0.85, (d) between 0.4 and 0.55 and between 0.55 and 0.7, (f) between 0.4 and 0.55 and between 0.55 and 0.7, (g) between 0.55 and 0.7 and between 0.7 and 0.85, (g) between 0.4 and 0.55 whereas in the other intervals the sample size is between 10 to 60 samples.

3.3 Particle velocity

The following conclusions are drawn from Figure 6.

1. From Figure 6(a) it can be hard to distinguish the two velocity profiles. However as ωt increases the two velocity profiles begin to deviate from each other. In (c) it can be seen that the particle moves faster when it moves downward than when it moves upward. This is because the particle originates from low-velocity regions when it moves upward, and therefore it will, on average, have relatively lower velocity, and vice versa. This behavior was also observed in Sumer and Deigaard, 1981, steady boundary layer experiments in an open channel. We note that, for some of the upper points (for high values of y) the data points in Figure 6 deviate from the general trends, because of a lower sample size for these upper positions.

2. Figure 6 shows clearly that the particle velocities are always smaller than the fluid velocities at the same elevation, as expected. This result is also in accord with Sumer and Deigaard (1981, Figure 7).

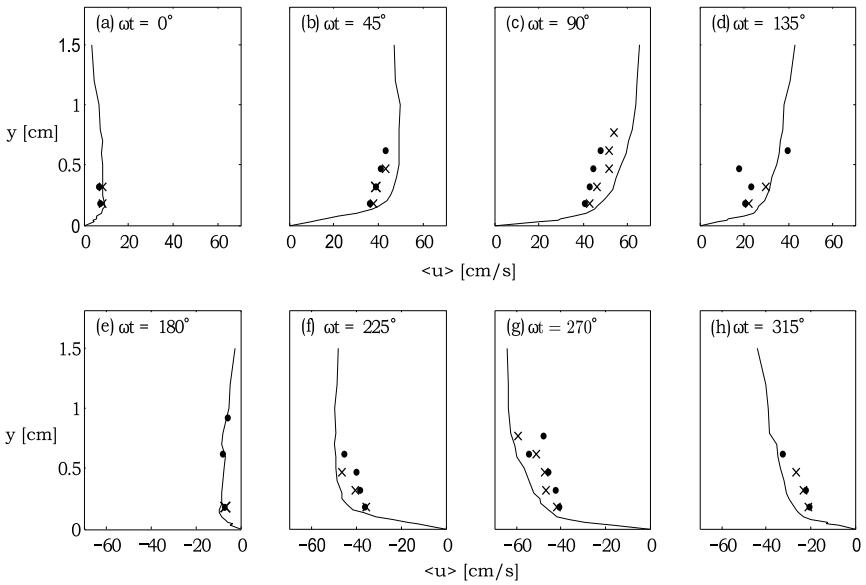

Figure 6. Velocity profile for the flow (only in the boundary layer); ×, $<u>$ for $v < 0$; •, $<u>$ for $v > 0$. The particle moves faster (save the phases $\omega t = 0^\circ$ and $\omega t = 180^\circ$) when it moves downward ($v<0$) and slower when it moves upward ($v>0$). For sample size see Figure 5.

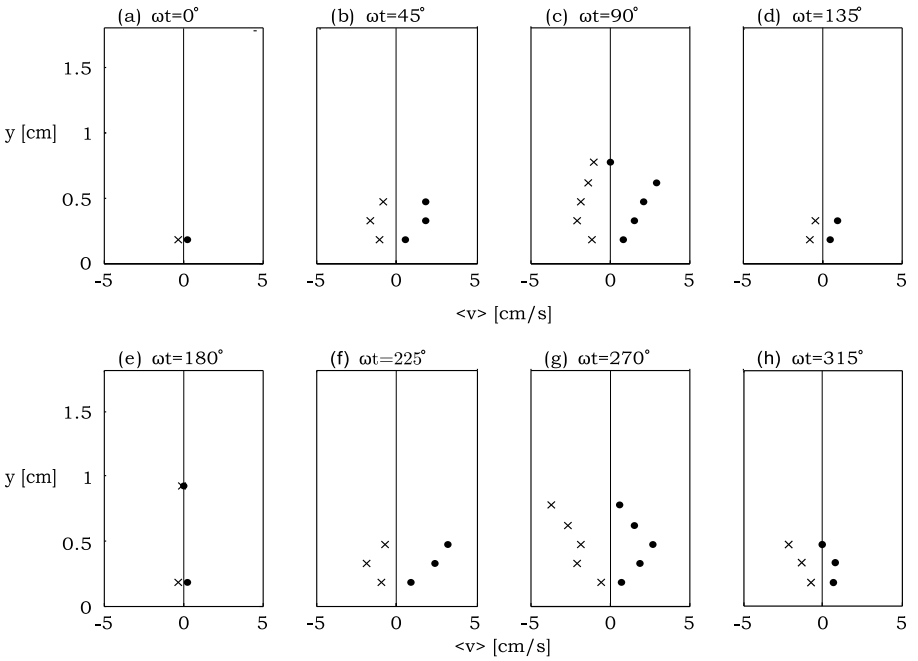

Figure 7. ×,$<v(v<0)>$; •, $<v(v>0)>$. The intervals are the same as on figure 3. Around flow reversal the particle is near the bed. Towards $\omega t = 90^\circ$ and 270° the particle move higher up. It can be seen that near the bed and the top of the profiles the velocities are lower than in the intervals in the middle. For sample size see Figure 5.

Figure 7 presents the conditional averaged vertical velocities of the particle, $<v(v>0)>$ and $<v(v<0)>$. The former quantity $<v(v>0)>$ is the mean vertical velocity of the particle corresponding to upward paths of the particle, and the second quantity $<v(v<0)>$ is the mean vertical velocity of the particle corresponding to downward paths of the particle.

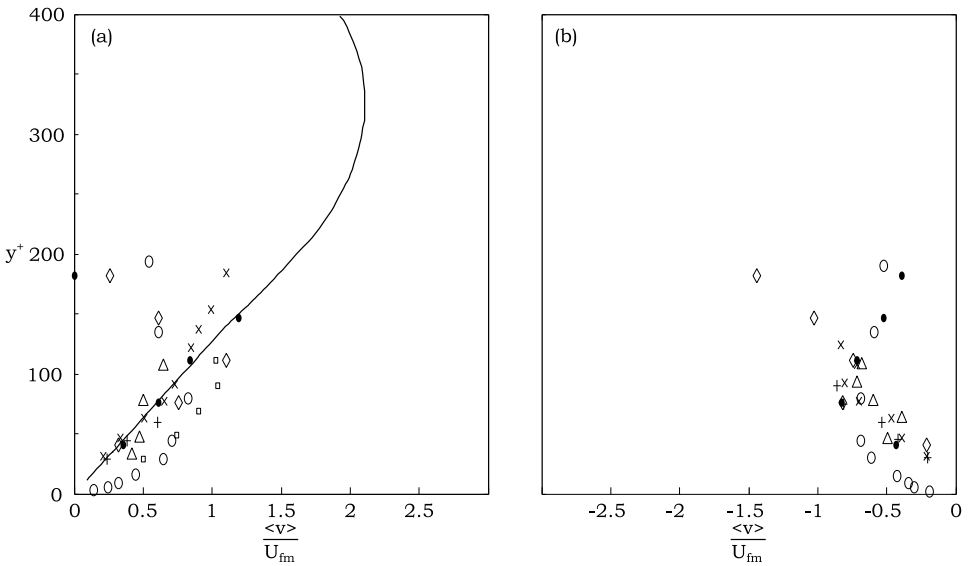

Figure 8. Reproduced from Sumer and Deigaard, (1981 figure 8 and 9) and the present results added. The conditional averaged vertical velocity for ωt = 90˚ and ωt = 270˚ where the oscillatory motion resembles a steady boundary layer flow due to the zero pressure gradient in the oscillatory boundary layer. The vertical scale is $y^+ = yU_{fm}/\nu$. (a) Upward directed motion. •, present test for ωt = 90˚; ◊, present test for ωt = 270˚; □ Sumer and Oguz, 1978; Δ, particle A, Sumer and Deigaard, 1981; x, particle B, Sumer and Deigaard, 1981; +, particle C Sumer and Deigaard, 1981; ——, Grass, 1974; ○, Brodkey et al., 1974. (b) Downward directed motion. •, present test for ωt = 90˚; ◊, present test for ωt = 270˚; Δ, particle A, Sumer and Deigaard, 1981; x, particle B, Sumer and Deigaard, 1981; +, particle C Sumer and Deigaard, 1981; ○, Brodkey et al., 1974.

From Figure 7, it can be seen that the vertical velocity increases as the flow accelerates ($\omega t \longrightarrow$ 90˚and $\omega t \longrightarrow$ 270˚). Furthermore, the velocity is low near the bed and then it increases until it starts to decrease again higher up in the flow for the upper intervals of the particle positions.

Figure 8 presents the data from Figure 7 normalized by the inner flow parameters for two phase values, namely ωt=90˚ (Figure 8(a)) and ωt=270˚ (Figure 8(b)). The figure also includes the data compiled by Sumer and Deigaard, 1981, for steady boundary layers (from Brodkey et al., 1974, Grass, 1974, Sumer and Oguz, 1978) plus their own data for comparison. Note that the present ωt=90˚ data covers the phase interval ωt = 80˚- 100˚ while the data corresponding to ωt=270˚ covers the phase interval ωt = 260˚- 290˚. The steady boundary layer data plotted in Figure 8 is essentially reproduced from Figures 7 and 8 of Sumer and Deigaard, 1981. Although there is scatter, discussed earlier, the results seem to agree with the steady boundary layer results.

4. Conclusion

By utilizing particle tracking, particle position has been determined of a particle released in an oscillatory flow in an oscillating tunnel. The statistics related to particle position is a function of the phase of the oscillatory flow**.** During the flow reversals, the particle stays near the bed. Otherwise the particle can reach heights as large as 2.5*d*-3*d* from the bed. The horizontal and vertical particle velocities are conditional averaged based on whether the particle moves up or down. The streamwise particle velocity is smaller when the particle moves up than when it moves down. The vertical velocity reveals that near the bed it approaches zero and then it increases before it assumes smaller values. It eventually tends to zero in the upper layers. The vertical velocity normalized by inner flow parameters around phases $\omega t = 90^{\circ}$ and $\omega t = 270^{\circ}$ compares favorably well with the results from the steady boundary layer research.

5. References

BRODKEY, R. S., WALLACE, J. M. & ECKELMANN, H. 1974. Some properties of truncated turbulence signals in bounded shear flows, *J. Fluid Mech.*, 63, 209

CARSTENSEN S., SUMER B. M. & FREDSØE J. 2010. Coherent structures in wave boundary layers. Part 1: Oscillatory motion, *J. Fluid Mech.*, 646, 169-206

GRASS, A. J. 1974. Transport of fine sand on a flat bed: turbulence and suspension mechanics, *Euromech.*, 48, Inst. Hydrodyn. Hydraulic Engng. Tech. Univ. of Denmark, p33.

HANRATTY T. J. & CAMPBELL J. A. 1982. Measurements of wall shear stress (ed. R. J. Goldstein), Hemisphere

HINO, M., SAWAMOTO, M. & TAKASU, S. 1976. Experiments on transition in an oscillatory pipe flow. *J. Fluid Mech.*, 75, 193-207

JENSEN B. L., SUMER B. M. & FREDSØE J. 1989. Turbulent oscillatory boundary layers at high Reynolds numbers, *J. Fluid Mech.*, 206, 265-297

NIÑO Y. & GARCIA M. H. 1996. Experiments on particle-turbulence interactions in the near wall-region of an open channel flow: implications for sediment transport, *J. Fluid Mech.*, 326, 285-319

PASTOR, M, 03 Oct 2012, Downloaded 2013-04-14 at :http://www.mathworks.com/matlabcentral/fileexchange/13840-simple-particle-tracking

SLEATH, J. F. A. 1987, Turbulent oscillatory flow over rough beds. *J. Fluid Mech.*, 182, 369-409

SUMER, B. M., ARNSKOV, M. M., CHRISTENSEN, N. & JØRGENSEN, F. E. 1993. Two-component hot-film probe for measurements of wall shear stress, *Experiments in Fluids*, 15, 380-384

SUMER, B. M. & DEIGAARD, R. 1981. Particle motion near the bottom in turbulent flow in an open channel. Part 2, *J. Fluid Mech.*, 109, 311-337

SUMER, B. M. & OGUZ, B. 1978. Particle motion near the bottom in turbulent flow in an open channel, *J. Fluid Mech.*, 86, 109-127